Structural intermediates in the assembly of taxoidinduced microtubules and GDP-tubulin double rings: Timeresolved X-ray scattering

ARTICLE *in* BIOPHYSICAL JOURNAL · JUNE 1996

Impact Factor: 3.97 · DOI: 10.1016/S0006-3495(96)79809-0 · Source: PubMed

5 AUTHORS, INCLUDING:

Jose Manuel Andreu
Centro de Investigaciones Biológicas
166 PUBLICATIONS **5,748** CITATIONS

SEE PROFILE

Structural Intermediates in the Assembly of Taxoid-Induced Microtubules and GDP-Tubulin Double Rings: Time-Resolved X-Ray Scattering

J. Fernando Díaz,* Jose M. Andreu,* Greg Diakun,‡ Elizabeth Towns-Andrews,‡ and Joan Bordas‡
*Centro de Investigaciones Biológicas C.S.I.C., Velazquez 144, 28006 Madrid, Spain, and ‡Daresbury Laboratory, Warrington WA4 4AD England

ABSTRACT We have studied the self-association reactions of purified GDP-liganded tubulin into double rings and taxoid-induced microtubules, employing synchrotron time-resolved x-ray solution scattering. The experimental scattering profiles have been interpreted by reference to the known scattering profiles to 3 nm resolution and to the low-resolution structures of the tubulin dimer, tubulin double rings, and microtubules, and by comparison with oligomer models and model mixtures. The time courses of the scattering bands corresponding to the different structural features were monitored during the assembly reactions under varying biochemical conditions. GDP-tubulin essentially stays as a dimer at low Mg^{2+} ion activity, in either the absence or presence of taxoid. Upon addition of the divalent cations, it associates into either double-ring aggregates or taxoid-induced microtubules by different pathways. Both processes have the formation of small linear (short protofilament-like) tubulin oligomers in common. Tubulin double-ring aggregate formation, which is shown by x-ray scattering to be favored in the GDP- versus the GTP-liganded protein, can actually block microtubule assembly. The tubulin self-association leading to double rings, as determined by sedimentation velocity, is endothermic. The formation of the double-ring aggregates from oligomers, which involves additional intermolecular contacts, is exothermic, as shown by x-ray and light scattering. Microtubule assembly can be initiated from GDP-tubulin dimers or oligomers. Under fast polymerization conditions, after a short lag time, open taxoid-induced microtubular sheets have been clearly detected (monitored by the central scattering and the maximum corresponding to the J_n Bessel function), which slowly close into microtubules (monitored by the appearance of their characteristic J_0, J_3, and J_{n-3} Bessel function maxima). This provides direct evidence for the bidimensional assembly of taxoid-induced microtubule polymers in solution and argues against helical growth. The rate of microtubule formation was increased by the same factors known to enhance taxoid-induced microtubule stability. The results suggest that taxoids induce the accretion of the existing Mg^{2+}-induced GDP-tubulin oligomers, thus forming small bidimensional polymers that are necessary to nucleate the microtubular sheets, possibly by binding to or modifying the lateral interaction sites between tubulin dimers.

INTRODUCTION

Mg^{2+} ions induce an isodesmic self-association of purified tubulin leading to the formation of characteristic double rings. The association equilibrium of the protein has been thoroughly analyzed by sedimentation velocity, and it has been shown that ring closure is favored in the GDP-liganded form rather than in the GTP-liganded form of tubulin (Frigon and Timasheff, 1975a,b; Howard and Timasheff, 1986; Shearwin and Timasheff, 1992). Under appropriate and very similar solution conditions, purified tubulin self-assembles into microtubules, which are the biologically relevant polymers of this protein (Lee and Timasheff, 1975; Hyams and Lloyd, 1994). The connection between the Mg^{2+}-induced formation of tubulin rings or microtubules is illustrated by the scheme shown in Fig. 1. The active form of the protein, GTP-tubulin, is converted in the wall of microtubules into GDP-tubulin, which is the inactive form of the protein. GTP hydrolysis does not occur upon ring formation. Microtubules are held together by interaction with fluctuating terminal caps of nonhydrolyzed GTP-tubulin and undergo dynamic instability (Erickson and O'Brien, 1992; Martin et al., 1993; Drechsel and Kirschner, 1994). It should be noted here that both rings and microtubules are stabilized by multivalent interactions with the microtubule-associated proteins (Melki et al., 1989; Butner and Kirschner, 1991; Novella et al., 1992; Mandelkow and Mandelkow, 1995) and that tubulin oligomers participate in the various tubulin association processes indicated (not shown in Fig. 1; Bordas et al., 1983; Spann et al., 1987; Melki et al., 1988, 1989; Mandelkow et al., 1988).

Taxoid antitumor drugs (Horwitz, 1994; Kingston, 1994; Rowinsky and Donehower, 1995) are often employed to stabilize microtubules in various experimental applications, for example, in the study of microtubule motor proteins (Gilbert et al., 1995; Hoenger et al., 1995; Kikkawa et al., 1995; Hirose at al., 1995). Ligands that bind to the taxoid site of microtubules constitute the only currently known agents capable of inducing the assembly of even the inactive GDP-tubulin into microtubules (see Fig. 1; Díaz and An-

Received for publication 21 August 1995 and in final form 23 January 1996.

This paper is dedicated to Professor Serge N. Timasheff on the occasion of his 70th birthday.

Address reprint requests to Dr. Jose M. Andreu, Centro de Investigaciones Biológicas C.S.I.C., Velazquez 144, 28006 Madrid, Spain. Fax: 34-1-5627518; E-mail: cibjm07@cc.csic.es; or to Dr. Joan Bordas, whose present address is Department of Physics, Liverpool University, P.O. Box 147, Liverpool L69 3BX, England. Fax: 44-151-7943441.

Dr. Díaz's present address is Laboratory of Chemical and Biological Dynamics, Katholieke Universiteit Leuven, Celestijnenlaan 200D, B-3001 Leuven, Belgium. Fax: 32-16-327982.

0006-3495/96/05/2408/13 $2.00

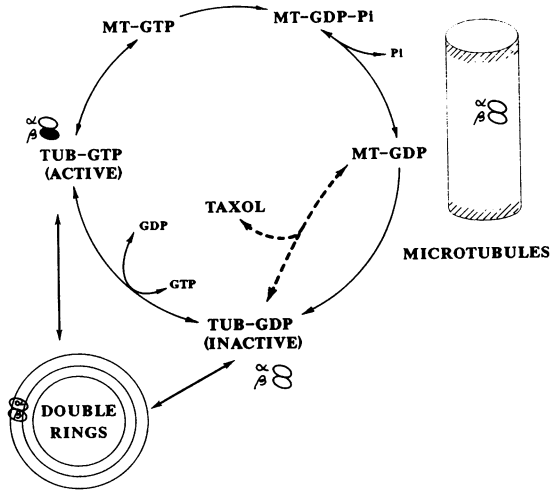

FIGURE 1 Scheme of the Mg^{2+}-induced assembly processes of tubulin. Note that taxol also enhances the assembly of GTP-tubulin and binds to assembled microtubules (not shown).

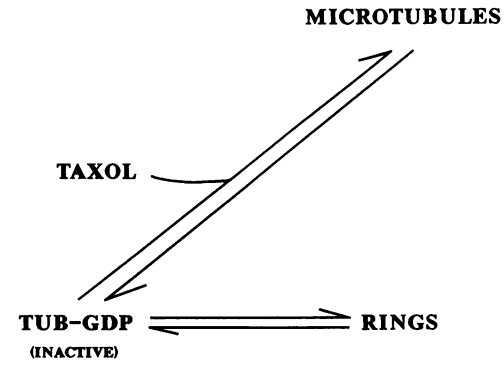

FIGURE 2 Scheme of the simplified model reactions of ring and microtubule assembly employed in this work.

dreu, 1993; Bollag et al., 1995). Taxoids probably block cell division by suppressing microtubule dynamic instability (Derry et al., 1995). The thermodynamics of the polymerization of taxoid-induced microtubules indicate that elongation is coupled to the binding of exactly one ligand molecule per assembled tubulin heterodimer, which stabilizes the microtubules (Howard and Timasheff, 1986; Díaz et al., 1993).

We have previously used synchrotron x-ray scattering methods to characterize the solution structure of microtubules induced by taxol and docetaxel to 3 nm resolution (Andreu et al., 1992, 1994), as well as the structure of GDP-tubulin double rings (Dáz et al., 1994). Both types of polymers constitute well-defined and simplified model systems of tubulin assembly. As indicated by the scheme shown in Fig. 2, both polymers can be considered to arise from global equilibrium reactions that have the GDP-tubulin dimer as a common reference state in the thermodynamic and structural sense. Here, we focus on the determination of the structural intermediates and the pathways of self-association of purified GDP-tubulin into double rings and taxoid-induced microtubules. The kinetics of these assembly reactions has been analyzed within the framework of the scheme in Fig. 2 by time-resolved x-ray scattering. Shifts in equilibrium have been induced by an increase in temperature, and the system has been examined as a function of the concentration of Mg^{2+}, of the degree of GDP substitution into the exchangeable nucleotide-binding site of tubulin, and of taxol or docetaxel ligand.

MATERIALS AND METHODS

GTP, dilithium salt, was from Boehringer; GDP, disodium salt, was from Pharmacia (ultrapure) or Boehringer. Taxol (paclitaxel; 4,10-acetoxy-2α-(benzoyloxy)-5β, 20-epoxy-1,7β-dihydroxy-9-oxotax-11-en13α-yl-(2*R*, 3*S*)-3-[(phenylcarbonyl)amino]-2-hydroxy-3-phenylpropionate; Bristol-Myers Squibb) and docetaxel (Taxotere; a side-chain analog of 10-deacetyl-taxol,4-acetoxy-2α-(benzoyloxy)-5β,20-epoxy-1,7β,10β-trihydroxy-9-oxotax-11-en-13α-yl-(2*R*, 3*S*)-3-[(*tert*-butoxycarbonyl)amino]-2-hydroxy-3-phenyl-propionate; Rhône-Poulenc Rorer) were kindly provided by Dr. M. Suffness (NCI, National Institutes of Health, Bethesda, MD) and by Dr. J.-L. Fabre (Rhône Poulenc Rorer, Antony, France), respectively. For taxoid structure-activity relationships see Kingston (1994).

Purified calf brain tubulin was prepared with 95% GTP (GTP-tubulin), 85% GTP-15% GDP, 40% GDP-60% GTP, 85% GDP-15% GTP, or over 99% GDP at its E-site (GDP-tubulin). This was measured by high-performance liquid chromatography as described previously (Díaz and Andreu, 1993; 85% GTP-tubulin was obtained by the addition of 1 mM GTP to GDP-tubulin).

Time-resolved x-ray scattering measurements to 3 nm resolution were made at station 2.1 of the Daresbury Laboratory Synchrotron Radiation Source, and data were processed as described before (Andreu et al., 1989, 1992, 1994; Díaz et al., 1994). The temperature of the sample solution was measured with a thermocouple and recorded simultaneously with the scattering data. The half-rise of the temperature increase from 2°C to 37°C took approximately 20 s. The x-ray scattering data were acquired in 5-s time frames. Data were smoothed by averaging each frame with the two preceding ones and the two ensuing ones. For kinetic purposes, the intensity of the scattering maxima was determined as follows: a) regions containing a scattering band were selected from the initial or final (microtubule samples) x-ray scattering records; b) a background under the scattering bands was constructed by passing a straight line through the minima, defined by the average of five detector pixels, at each side of the band; c) this background was subtracted and the intensity of the remaining x-ray scattering band was calculated by integration.

The x-ray scattering profile models of tubulin assemblies were calculated by employing a solution scattering simulation program (DALAI; Pantos and Bordas, 1994) as previously described (Andreu et al., 1992; Díaz et al., 1994).

RESULTS

Fig. 3 shows x-ray scattering traces calculated from models that are relevant and necessary for the analysis of the data to be presented below. It will be shown how changes in solution conditions permit the dissection of different assembly reactions of tubulin and the detection of structural intermediates. Furthermore, by merging the various experimental observations, the assembly pathways of the GDP-tubulin dimer into double rings and microtubules will be formulated in the Discussion.

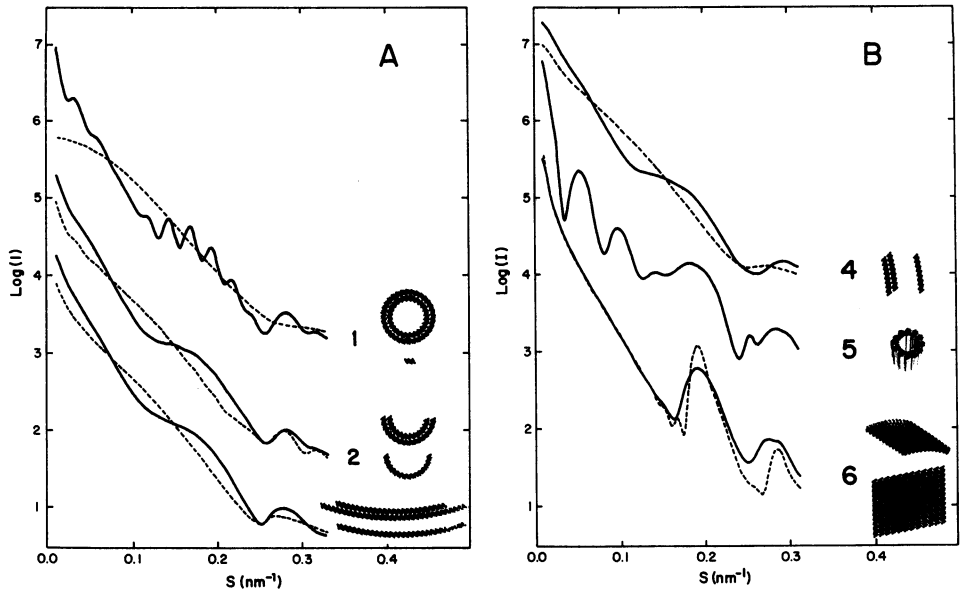

FIGURE 3 Computed x-ray solution scattering profiles of model tubulin assemblies. α- and β-tubulin have been represented by the same monomer previously employed in the modeling of the scattering profile of microtubules (Andreu et al., 1992, 1994), which consists of a set of closely packed spheres of 1.2 nm diameter within an approximately triaxial ellipsoidal envelope of 4 × 7 × 8 nm. (*A*) Dashed line 1, $\alpha\beta$-tubulin dimer; solid line 1, tubulin double ring made of 32 and 24 monomers (Díaz et al., 1994); curve 2, solid line, half double ring; curve 2, dashed line, half single ring (14 monomers); curve 3, solid line, tubulin double ring opened to a 30° circumference arc; curve 3, dashed line, the same but single ring (28 monomers). (*B*) Curves 4, tubulin oligomers consisting of 8-monomer-long fragments of the respective models in curves 3; curve 5, model of microtubule population (Andreu at al., 1994) consisting of 30% 13 protofilament microtubules, 40% 12 protofilament microtubules, 30% 11 protofilament microtubules, each of them cylindrically closed; curve 6, dashed line, 12 protofilament three start opened flat microtubular lattice, modeled as described (Andreu et al., 1992); curve 6, continuous line, same, but partially rolled onto a 30° cylindrical sector.

Assembly and disassembly of GDP-tubulin double-ring aggregates

Fig. 4 shows the x-ray scattering profiles of GDP-tubulin at varying Mg^{2+} concentrations. These results are readily interpreted by reference to the x-ray scattering profiles yielded by tubulin double-ring pseudolattices at the same resolution (Díaz et al., 1994) and by comparison to the models (Fig. 3). The x-ray scattering traces of tubulin preparations without added Mg^{2+} (Fig. 4, *trace 1*) corresponds to those expected from tubulin dimers. The pattern at 4 mM $MgCl_2$ (Fig. 4, *trace 2*) is featureless, but relative to that without Mg^{2+} it displays a significant increase in intensity at low angles. This indicates the presence of a significant proportion of tubulin oligomers. The x-ray scattering traces obtained at higher Mg^{2+} concentrations show a noticeable increase in the proportion of tubulin double rings in the solutions. This is clearly shown by the enhancement in the scattered intensities at very low angles, which is proportional to the overall degree of polymerization, and by the development of the x-ray scattering features characteristic of double rings. These consist of scattering bands following the sequence of a J_0-like Bessel function and are prominent in traces 3 and 4 of Fig. 4 and in the band at 0.28 nm^{-1}. The latter is due to the disposition of tubulin subunits along the ring perimeter and corresponds to a J_n Bessel function, where n is the number of subunits. The prominence of these features reaches a maximum at about 7 to 11 mM total Mg^{2+} (see *inset* in Fig. 4). In addition, a diffraction band at 0.026 nm^{-1} also develops with increasing Mg^{2+} concentration. This feature is due to the formation of a pseudolattice of rings (Díaz et al., 1994) and always coexists with those due to the presence of double rings. At higher (17 mM) Mg^{2+} concentrations, GDP-tubulin solutions precipitated as previously reported (Diaz and Andreu, 1993), and the x-ray scattering profiles showed far fewer regular features.

Fig. 5 shows the x-ray scattering profiles of solutions of GTP-tubulin and GDP-tubulin with different degrees of nucleotide substitution, at a constant 7 mM $MgCl_2$ concentration. The x-ray scattering traces of GTP-tubulin samples (*curves 1* and *5*) are of the type expected from solutions that contain a majority of linear tubulin oligomers as shown by comparison with the model calculations 2, 3, and 4 (*dashed lines*) in Fig. 5. At the tubulin concentrations attained in this experiment, the characteristic double-ring features and the peak at 0.28 nm^{-1} were apparent with 85% to 99% exchange of GDP (Fig. 5, *curves 3* and *4*, respectively). Examination of GTP-tubulin and partially exchanged GDP-tubulin samples (Fig. 5, *traces 1* and *2*) by sedimentation velocity showed an asymmetrical sedimentation boundary, with a characteristic strong bimodality in GDP-tubulin (Fig. 5, *inset B*). Addition of GTP to GDP-tubulin, which gives back-exchanged GTP-tubulin, decreased the x-ray scattering features characteristic of rings to their initial level (compare *curves 5* and *1* in Fig. 5). Furthermore,

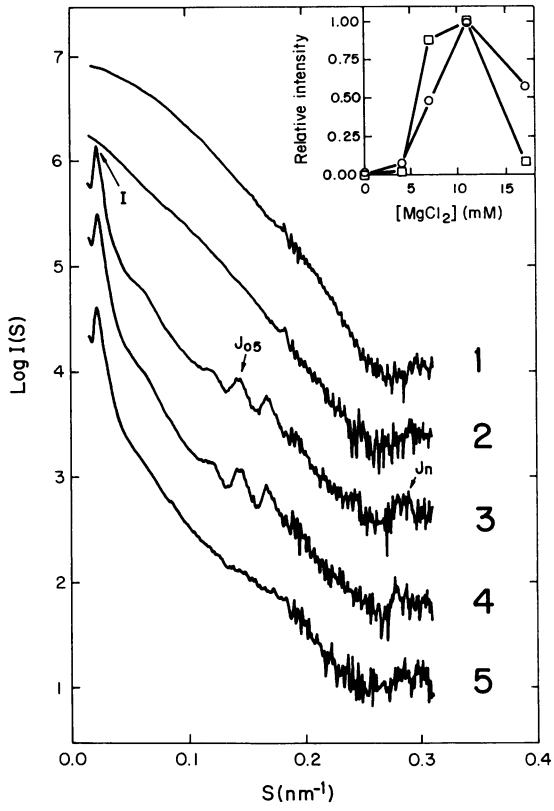

FIGURE 4 X-ray scattering profiles of GDP-tubulin in PEDTA (10 mM phosphate, 1 mM (ethylenediamine)tetraacetic acid), 1 mM GDP (pH 6.7) at 2°C and different $MgCl_2$ concentrations. Curve 1, 125 μM tubulin, 0.5 mM $MgCl_2$; curve 2, 95 μM tubulin, 4 mM $MgCl_2$; curve 3, 85 μM tubulin, 7 mM $MgCl_2$; curve 4, 75 μM tubulin, 11 mM $MgCl_2$; curve 5, 60 μM tubulin, 17 mM $MgCl_2$. The inset shows the intensities of the interference peak (labeled I) (○), and the 5th subsidiary maxima of the J_0-like ring Bessel function (labeled J_{05}) (□) of the profiles as a function of the $MgCl_2$ concentration and expressed relative to the maximum value.

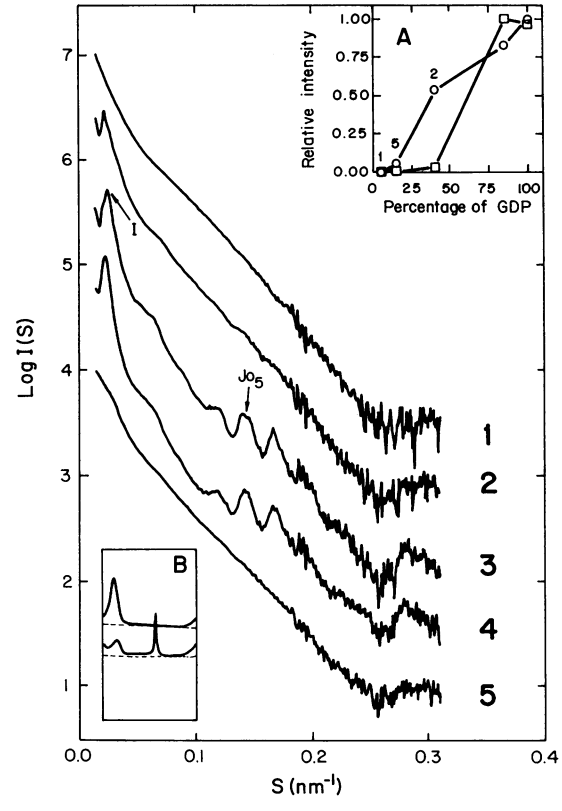

FIGURE 5 X-ray scattering profiles of the Mg^{2+}-induced association products of GTP- and GDP-tubulin at 2°C, at different degrees of nucleotide exchange. Profile 1, 135 μM tubulin equilibrated in 10 mM phosphate 6 mM $MgCl_2$ (pH 6.7), 1 mM GTP added (95% GTP-tubulin, 5% GDP-tubulin); profile 2, 135 μM tubulin equilibrated in 10 mM phosphate, 6 mM $MgCl_2$ (pH 6.7), 1 mM GDP added (40% GDP-tubulin); profile 3, 75 μM tubulin equilibrated in PEDTA 1 mM GDP (Boehringer), 7 mM $MgCl_2$ added (pH 6.7) (85% GDP); profile 4, 85 μM tubulin equilibrated in PEDTA 1 mM GDP (Pharmacia), 7 mM $MgCl_2$ added (pH 6.7) (99% GDP); profile 5, as sample 4, but after addition of 1 mM GTP (85% GTP-tubulin, 15% GDP-tubulin). (*Inset A*) Relative intensities of the interference peak (○) and the 5th subsidiary maxima of the J_0 Bessel function (□) of the curves as a function of the percentage of GDP. (*Inset B*) Sedimentation velocity Schlieren profiles of 80 μM tubulin equilibrated in 10 mM sodium phosphate, 6 mM $MgCl_2$, to which either 1 mM GTP (*upper profile*, GTP-tubulin as in curve 1) or 1 mM GDP (*lower profile*, 40% GDP-tubulin as in curve 2) was added. Both samples were loaded into a double-sector cell and centrifuged at 48,000 rpm and 20°C in an AnD rotor in a Beckman model E analytical ultracentrifuge (picture taken at minute 19 and bar angle 65°). The uncorrected sedimentation coefficients determined were 6.6 S for GTP-tubulin, and 8.1 S and 31 S for the slow and fast peaks of GDP-tubulin, respectively.

under these conditions, the turbidity characteristic of the double-ring aggregates disappeared in less than 1 min after GTP addition in the cold (Díaz and Andreu, 1993).

Fig. 6 *A* illustrates the effects of a temperature increase from 2°C (*curve 1*) to 37°C (*curves 2* to *5*) on the x-ray scattering by GDP-tubulin ring aggregates in 7 mM $MgCl_2$. Increasing the temperature results in a marked decrease of the interference peak and the J_0-like Bessel function bands, but only in a modest change in the shape of the J_n maximum. These results clearly indicate a destabilization of the double-ring structure, but the persistence of the J_n scattering band implies that the contacts between tubulin monomers along the ring perimeter are still present. In fact, comparison with the model scattering profiles (Fig. 3) shows that the scattering profile at 37°C (Fig. 6, *curve 5*) can be explained as being due to either a majority of halved rings (Fig. 3, *curve 2*) or open rings (*curve 3*) or to small fragments of them (*curve 4*). Note that these three types of structures yield essentially indistinguishable x-ray scattering profiles within the current precision of our measurements. As shown by the dashed line 5 in Fig. 6, the experimental profile can be approximately reproduced by a mixture of small ring fragments with residual double rings. It is clear from the complete absence of any of their characteristic x-ray scattering features that microtubules are not formed in these conditions. Fig. 6 *B* shows the time courses of the interference peak and the J_{05}-like maximum resulting from the warming of the sample. These may be compared with the turbidity time course shown by the inset of Fig. 6 *A*. The intensities of these scattering features exhibit an initial rapid decrease that is simultaneous with that of the turbidity

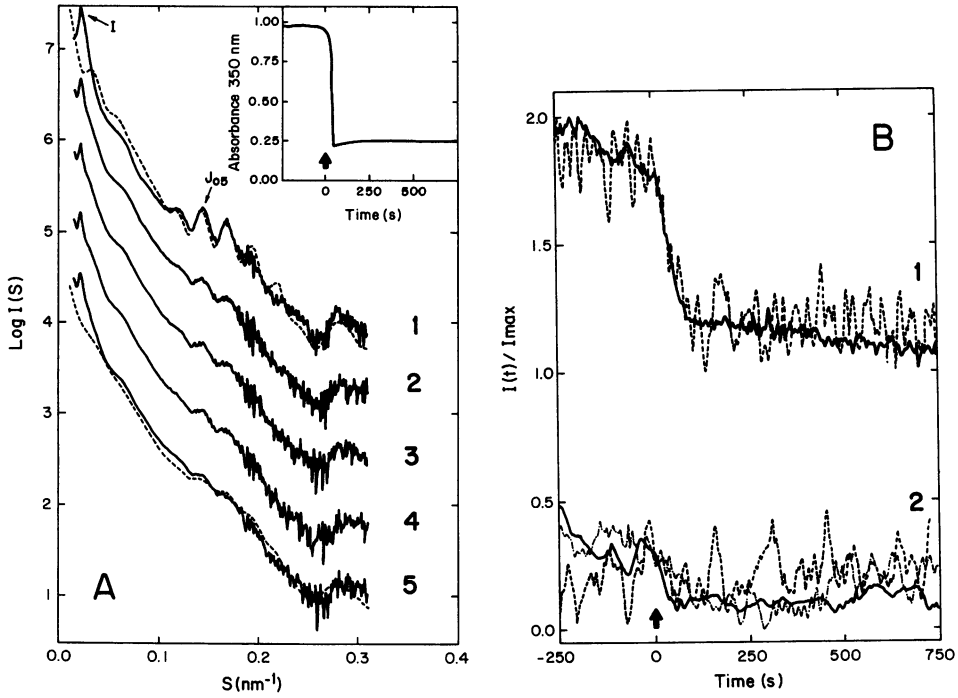

FIGURE 6 Effect of temperature on the self-association of 85 μM GDP-tubulin in PEDTA, 1 mM GDP, 7 mM $MgCl_2$ (pH 6.7). (*A*) Curve 1, solid line, x-ray scattering profile at 2°C (the dashed line 1 is the ring scattering model 1 from Fig. 1); curves 2–5, average profiles after a temperature shift to 37°C; curve 2, second 0 to 250; curve 3, second 500 to 750; curve 4, second 750 to 1000; curve 5, second 1400 to 2000; the dashed line 5 corresponds to 80% model single linear oligomers and 20% model double rings (from models 4 and 1, respectively, in Fig. 1). (*Inset*) Time course of turbidity (60 μM GDP-tubulin). (*B*) Solid line 1, time course of the intensity of the ring interference peak I during the experiment in *A*; dashed line 1, time course of the ring J_{05}-like Bessel function peak; lines 2, time course of intensity of the central scattering and of the scattering vector intervals that would correspond to the J_{02} and J_{12} microtubule signals (see Fig. 7).

signal. These changes, which occur in about 1 min, are readily interpreted as being due to a substantial reduction in the amount of double-ring arrays in the solution. Subsequently the x-ray features show a much slower rate of decrease while the turbidity remains constant (as shown by inspection of profiles 2 to 5 in Fig. 6 *A*). When the total Mg^{2+} concentration was increased to 11 mM the ring sheets only partially disassembled upon warming. It should be noted that some tubulin preparations required 10 to 12 mM Mg^{2+} for optimal reversible double-ring formation.

Once the GDP-tubulin double ring pseudolattices were dissociated at 37°C, and their temperature were subsequently reduced back to 2°C, the reassembly of the ring arrays was a slow process. This reassembly was markedly sped up by the addition of equimolar taxol or docetaxel (not shown). The final positions and intensities of the x-ray scattering maxima from these samples were identical to the initial GDP-tubulin samples without taxoid (Fig. 6). This suggested a possible taxoid effect on the formation of the double-ring aggregates. However, the self-association behavior of 40% exchanged GDP-tubulin leading to double-ring formation, as monitored by their characteristic bimodal sedimentation velocity profile, was not significantly modified by taxol addition to one of two identical aliquots run in parallel in a double-sector cell at 2°C. It was observed that the area under the fast peak at 2°C was smaller than at 20°C, which is consistent with an endothermic association process (data not shown).

Time courses of microtubule assembly from tubulin rings, oligomers, or dimers

The warming of GDP-tubulin in 7 mM $MgCl_2$ with equimolar taxoid (either taxol or docetaxel) first induced the dissociation of the double-ring sheets, which was followed by the assembly of microtubules. The time-averaged x-ray scattering profiles shown in Fig. 7 *A* illustrate these effects. Fig. 7 *B* shows the time courses of the various x-ray scattering signals. The initial scattering trace at 2°C and the fast dissociation phase of the ring aggregates are indistinguishable from those observed without taxoid (Fig. 6). However, as the ring signals approach their maximum decrease, the bands following a J_0 and J_n Bessel function, which are characteristic of the presence of microtubules in the solution (Andreu et al., 1992; compare to models in Fig. 3), began to grow (Fig. 7 *B*, *dash-point* and *dashed lines*, respectively). The final scattering profile is that expected from a solution containing a majority of microtubules. Nevertheless, some residual double-ring arrays are still present, as indicated by their characteristic interference peak at very low angles (Fig. 7 *A*, *curve 5*). Identical measurements performed on an aliquot of the same solution but after the addition of 1 mM GTP showed much less developed ring features at 2°C, a faster growth of the microtubule signals immediately after warming, and full microtubule assembly in the final state (data not shown; the results are similar to those shown in Fig. 9). In the presence of 11 mM $MgCl_2$, where the ring aggregates of GDP-tubulin resist dissociation at 37°C, the taxoid-induced microtubule assembly occurred very slowly and only to a limited extent (not shown). On the other hand, lowering the cation concentration to 4 mM $MgCl_2$ minimized the formation of ring aggregates while it permitted microtubule assembly (Fig. 11). The most straightforward interpretation of these results is that the formation of ring aggregates competes with the microtubule assembly. Assembly of GDP-tubulin into microtubules without any significant interference due to the formation of ring aggregates

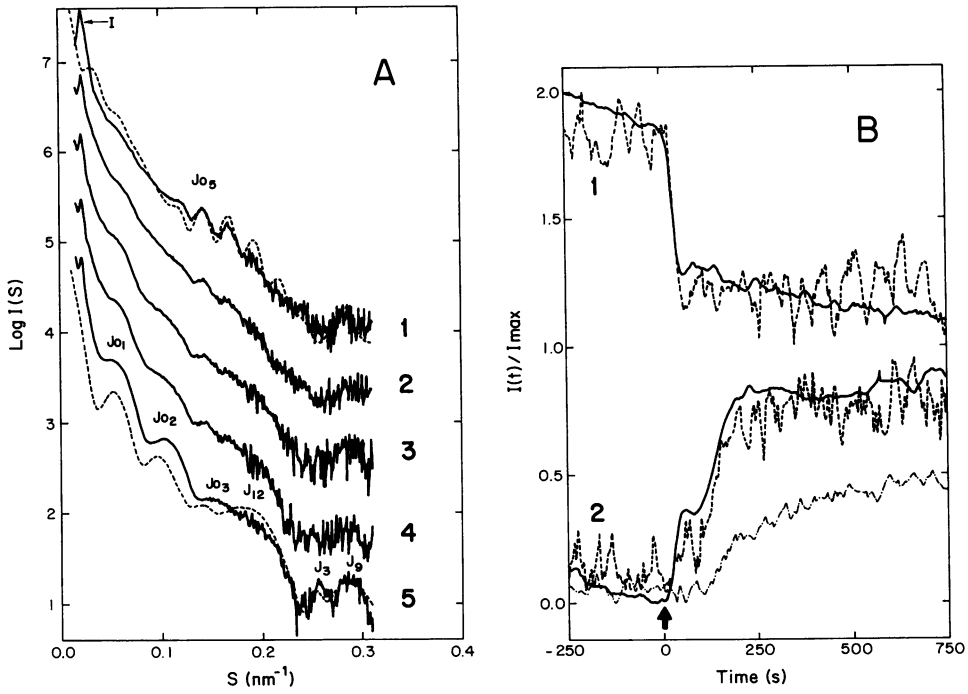

FIGURE 7 (*A*) X-ray scattering profiles during assembly of 75 μM GDP-tubulin-taxol in PEDTA, 1 mM GDP, 7 mM $MgCl_2$ (pH 6.7). Sample 1 is at 2°C (the dashed line is the double ring model 1 from Fig. 1); curves 2 to 5 are the average scattering profiles after a temperature shift to 37°C; curve 2, second 1–250; curve 3, second 250–500; curve 4, second 500–750; curve 5, second 1400–2000 (the dashed line is a combination of 5% double ring, 15% linear oligomer, and 80% microtubule scattering models from Fig. 1). (*B*) Time course of the ring and microtubule scattering signals during the experiment of *A*. The solid and dashed line 1 are the intensities of the interference peak I and the ring J_{05}-like peak, respectively. The solid, dashed, and dash-point line 2 are the intensities of the central scattering, and the microtubule J_{12} and J_{02} peaks, respectively. The intensity of each peak has been divided by its maximum value.

could be obtained by the addition of 7 mM $MgCl_2$ to a warm tubulin-taxoid solution. Taxol does not bind appreciably to tubulin dimers (Díaz et al., 1993), and hence it does not modify their scattering. As shown by Fig. 8 (*trace 1*), the initial scattering profile essentially corresponds to tubulin dimers, whereas Mg^{2+} addition to the solution rapidly induces microtubule polymerization (Fig. 8, *trace 2* and *inset*).

Assembly and closure of microtubule lattices from tubulin oligomers

Fig. 9 shows the time-averaged x-ray scattering profiles (Fig. 9 *A*) and the time course of the different scattering bands (Fig. 9 *B*) of a GTP-tubulin taxol solution undergoing assembly initiated by a temperature increase from 2°C to 37°C. The initial scattering profile is that expected from a solution with a majority of tubulin oligomers and incipient microtubule formation. Immediately after the temperature rise the central scattering and the J_{12} signals rise rapidly and simultaneously, whereas the J_0 peaks increase more slowly. A similar result was obtained with docetaxel. The consecutive scattering profiles can be approximately simulated by mixtures of oligomers and microtubules (Fig. 9, *inset*), whereas the final state corresponds to the presence of a majority of microtubules in the solution. Slowing the assembly process helped to resolve the rates of growth of the various structural features due to microtubules, while avoiding interference with the bands due to ring aggregates. This was accomplished by the preparation of 40% exchanged GDP-tubulin, rather than tubulin with 99% GDP at the E-site (Materials and Methods and Fig. 5, *profile 2*), and by immediate examination of its taxoid-induced assembly. The initial state at 2°C has fewer features, consisting of a broad maximum centered around 0.28 nm^{-1} and incipient double-ring J_0-like maxima (Fig. 10 *A*; the interference peak due to ring association is absent). As shown by Fig. 10 *B*, the J_{12} signal grows simultaneously with the central scattering shortly after (~20 s) the temperature increase. Approximately 30 s later the J_0 peaks start to develop, but they do so much more slowly than the central scattering. Although the noise at these angles prevented the accurate determination of the intensity time courses, the J_3 and J_9 helical peaks seemed to develop more slowly than the J_{12}, and paralleled the time course of the J_0 (Fig. 10 *A*). [Note that the solution scattering maximum at 0.250 nm^{-1} has been assigned to the J_3 fiber diffraction maximum of the first layer line, arising from electron density features in the direction of the three-start helix of the microtubule surface lattice (Andreu et al., 1992, 1994). It might also contain an overlapping contribution of a second subsidiary maximum of the equatorial J_n Bessel function (see, for example, figure 1 in Beese et al., 1987), whose relative contribution is not well defined. However, the maximum at 0.250 nm^{-1} evolves independently of the J_n maximum at 0.190 nm^{-1}, which suggests that most of its intensity has a nonequatorial origin. Furthermore, the practical identity in this region of the scattering profiles of microtubules induced by docetaxel and taxol, which have clearly different lower-angle J_0 maxima (Andreu et al., 1994), indicates a nonsignificant contribution of the fourth, etc., subsidiary maxima of the J_0 Bessel function.] Equivalent results were obtained by substituting docetaxel for taxol. These results can be readily interpreted by reference to the x-ray solution scattering of microtubules at this resolution (Andreu et al., 1992, 1994) and by comparison to the models in Fig. 3; the scattering profile at 4°C corresponds to

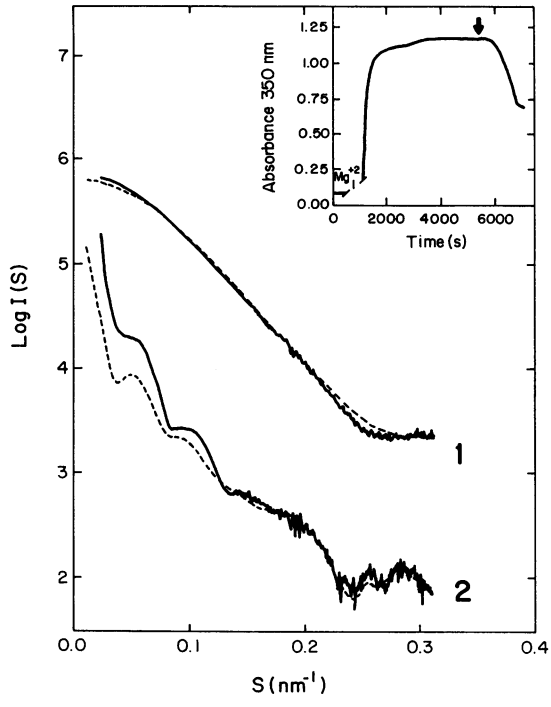

FIGURE 8 X-ray scattering traces of 80 μM GDP-tubulin-taxol in PEDTA, 1 mM GDP at 37°C before (*curve 1*) and 120 to 370 s after (*curve 2*; final pH 6.7) the addition of 7 mM $MgCl_2$. The dashed line 1 is the dimer scattering model 1 (Fig. 3). The dashed line 2 corresponds to 35% single linear oligomer and 65% microtubule models (Fig. 3). (*Inset*) Turbidity time course (47.5 μM GDP-tubulin-taxol)

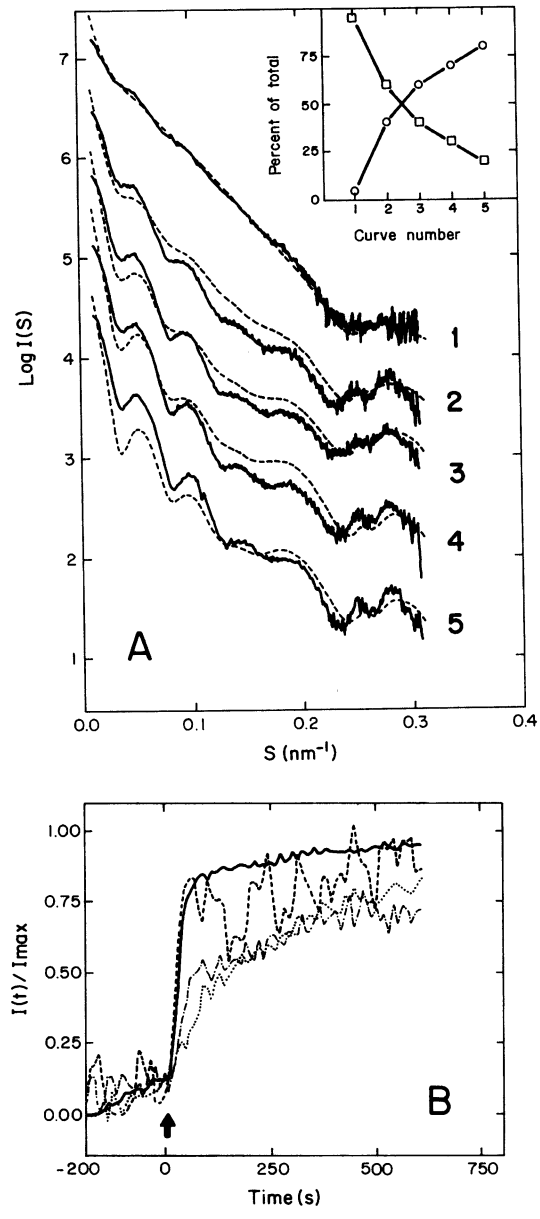

FIGURE 9 (*A*) X-ray scattering profiles during assembly of 200 μM GTP-tubulin-taxol in 10 mM phosphate, 1 mM GTP, 6 mM $MgCl_2$ (pH 6.7). Curve 1, at 2°C; curves 2 to 5, average scattering profiles between second 0–200, 200–400, 400–600, 1400–2000 after warming to 37°C. The dashed lines are model mixtures of single linear oligomers and microtubules (models 4 and 6, respectively, in Fig. 3). All possible mixtures of the two species in 5% steps were calculated, and those giving the least-squares deviation were selected. (*Inset*) Percentage of linear oligomers (□) and microtubules (○) employed to approximately model the scattering curves. (*B*) Solid, dash, point, and dash-point lines, respectively: time course of the intensities of the central scattering, J_{12}, J_{01}, and J_{02} peaks in the experiment of *A*.

tubulin oligomers and a few double rings. During the first 20 s after warming no large structures were detected, but small oligomers were observed in the solution (nucleation phase). Approximately between second 20 and second 50 open-sheet polymers with the characteristic organization of the microtubule wall were detected (Fig. 10 *B*; see also *profile 2* in Fig. 10 *A*), and these closed in a subsequent slow process (Fig. 10 *B* and *profiles 3* and *4* in Fig. 10 *A*) to give a majority of pseudohelical microtubules at equilibrium (*profile 5*). Approximate simulation of the different time averages in terms of mixtures of oligomers and microtubules requires the inclusion of open microtubule models as intermediate structures, the amount of which must first grow and later decrease (Fig. 10, *inset*). When the temperature is increased slowly, as shown by Fig. 10 *C*, the growth of the different microtubule peaks occurs simultaneously, indicating that under these conditions the bidimensional polymerization is slow enough to allow the cylinder closure to occur at a comparable speed, making it impossible to separate the two phenomena.

When we examined the effects of solution variables on taxoid-induced microtubule assembly kinetics, we found that the same modifications that enhance the taxoid-induced microtubule elongation equilibrium (Díaz et al., 1993) affect the kinetics of microtubule formation in a qualitatively similar manner. Fig. 11 *A* shows how increasing Mg^{2+} concentration reduces the lag time of polymerization and increases the rate of assembly. Fig. 11 *B* indicates that the substitution of docetaxel for taxol also reduces the lag time and increases the rate of microtubule assembly. Finally, Fig. 11 *C* compares GDP- and GTP-tubulin at 4 mM total Mg^{2+} concentration, in conditions where no noticeable ring for-

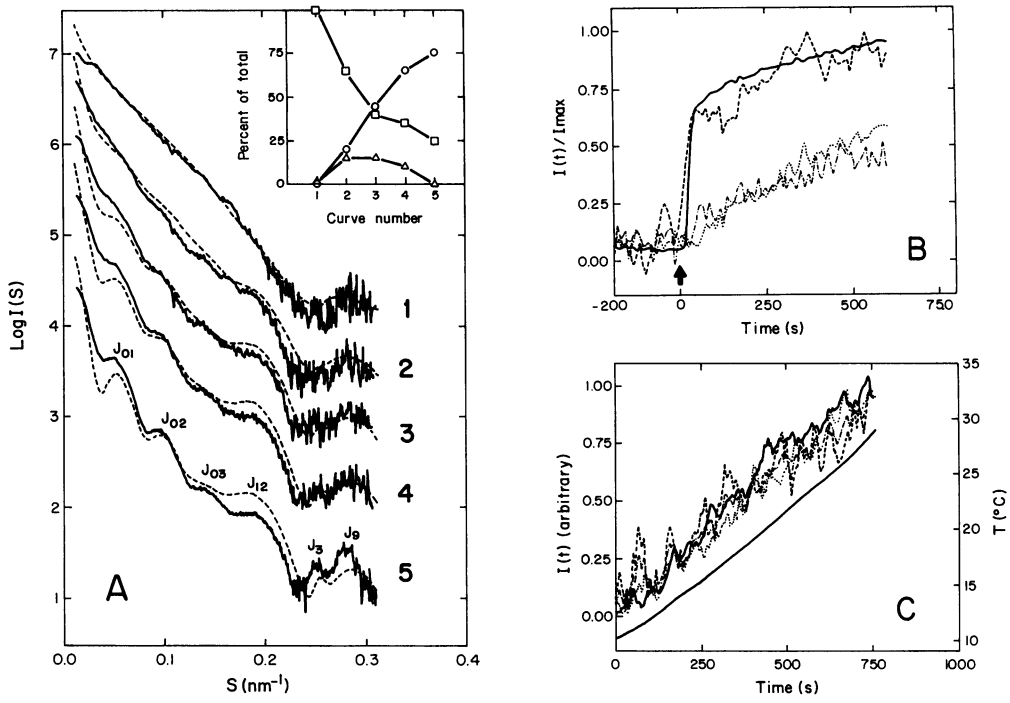

FIGURE 10 (*A*) X-ray scattering profiles during assembly of 200 μM (40% GDP)-tubulin-taxol in 10 mM phosphate, 1 mM GDP, 6 mM $MgCl_2$ (pH 6.7). Curve 1, at 2°C; curves 2 to 5, averages at second 0–200, 200–400, 400–600, and 1400–2000 after warming to 37°C. The dashed lines correspond to model mixtures of linear oligomers, microtubular sheets, and microtubules (models 4, 5, and 6, respectively, Fig. 3). All possible mixtures of the three species in 20% steps were calculated, and refined in 5% steps to give minimum least-squares deviation. (*Inset*) Percentage of linear oligomers (□), microtubules (○), and sheets (△) employed to model each curve. (*B*) Solid, dash, point, and dash-point lines, respectively: time course of the intensities of the central scattering, J_{12}, J_{01}, and J_{02} peaks in the experiment of *A*. (*C*) Time course of the corresponding intensities during assembly induced by a slow temperature crawl. Temperature is indicated by the lower solid line.

mation is induced. The presence of the nucleotide γ-phosphate slightly reduces the lag time of microtubule polymerization. It can also be observed in Fig. 11 *C* that, similarly to Fig. 10, the peak corresponding to the microtubule J_{02} Bessel function grows much more slowly than the central scattering.

DISCUSSION

The results described above show that the Mg^{2+}-induced processes of GDP-tubulin self-association either into double rings or taxoid-induced microtubules fit into a global scheme (Fig. 12), which is elaborated on below.

Tubulin double-ring assembly and disassembly

Solutions of purified calf brain GTP- or GDP-tubulin in our concentration range and without added cation exclusively contain the 5.8 *S* αβ dimer (Figs. 3 and 4; Andreu et al., 1989; García de la Torre and Andreu, 1994, and unpublished results). Addition of low concentrations of Mg^{2+} results in the formation of tubulin oligomers, but with little ring formation. Increasing Mg^{2+} concentrations in the absence of guanosine nucleotide γ-phosphate induces extensive formation of characteristic double-ring pseudocrystalline arrays (Figs. 1, 2, and 3; Díaz et al., 1994). These events correspond to processes 1 and 2 of the global scheme shown by Fig. 12. Process 1 consists of successive tubulin dimer self-association equilibria, forming linear oligomers of indefinite length (note that the degree of curvature of these oligomers has not been determined). In process 2 the oligomers close circularly and associate to form the well-defined double rings (note that the ring closure reaction is a unimolecular association), and the rings aggregate. The effects of the divalent cation and nucleotide on the ring formation observed by x-ray scattering are qualitatively fully consistent with the effects they have on the tubulin isodesmic self-association leading to the formation of the 42 *S* ring polymer, which have been measured in hydrodynamic studies (Frigon and Timasheff, 1975b; Howard and Timasheff, 1986; Shearwin and Timasheff, 1992). Our results are also consistent with the notion that GDP-tubulin forms the rings more easily than GTP-tubulin because it coils better (Howard and Timasheff, 1986; Melki et al., 1989; Díaz et al., 1994). Indeed, the reverse of process 2 (disassembly of ring arrays into oligomers) is achieved by back-exchange of GTP into its binding site (Fig. 5 *A*, *trace 5*).

The double rings assembled from GDP-tubulin aggregate into pseudolattices in the cold. For intermediate Mg^{2+} concentrations (~7–10 mM) these arrays and the double rings dissociate upon warming. X-ray scattering does not distin-

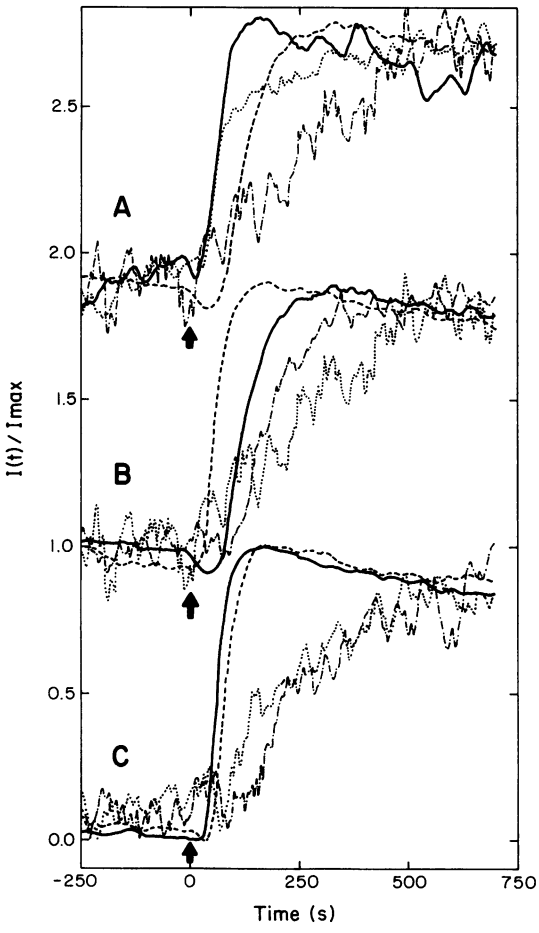

FIGURE 11 Time course of the intensities of central scattering and J_{02} peak during microtubule assembly with different Mg^{2+} concentrations, nucleotide and taxoid. (*A*) 95 μM GTP-tubulin in PEDTA, 1 mM GDP plus 1 mM GTP (pH 6.7); solid line, central scattering at 7 mM $MgCl_2$; dashed line, central scattering at 4 mM $MgCl_2$; dotted line, J_{02} at 7 mM $MgCl_2$; dash-dot line, J_{02} 4 mM $MgCl_2$. (*B*) 95 μM GTP-tubulin in PEDTA, 1 mM GDP plus 1 mM GTP, 4 mM $MgCl_2$ (pH 6.7); solid line, central scattering with taxol; dashed line, central scattering with docetaxel; dotted line, J_{02} with taxol; dash-dot line, J_{02} with docetaxel. (*C*) 85 μM tubulin in PEDTA, 1 mM GDP (GDP-tubulin), or 1 mM GDP plus 1 mM GTP (GTP-tubulin), 4 mM $MgCl_2$ (pH 6.7); solid line, central scattering of GTP-tubulin; dashed line, central scattering of GDP-tubulin; dotted line, J_{02} of GTP-tubulin; dash-dot line, J_{02} of GDP-tubulin.

guish well between the various ring dissociation products (they could be anything from small fragments to uncoiled rings; Figs. 3 and 6). However, once the cyclic polymers break up, the system is under a simple isodesmic polymerization regime, whose thermodynamic properties (Oosawa and Asakura, 1975; Frigon and Timasheff, 1975a,b) dictate that the species populated at equilibrium are the unassociated protein and small oligomers, with a negligible proportion of higher order oligomers. Therefore we favor the interpretation that the main species formed at 37°C are small ring fragments. Actually, it may be assumed that the species formed upon thermal ring disassembly are oligomers similar to those formed by the association of the tubulin dimer.

The above leads to an apparent thermodynamic paradox, which arises from the following experimental observations. The Mg^{2+}-induced self-association of GTP-tubulin leading to double-ring formation is clearly an endothermic process (Frigon and Timasheff, 1975b; results not shown). Furthermore, the bimodal sedimentation pattern and the cooperativity of the process, which are characteristic of the formation of a cyclic end-polymer, remain at a high temperature (Frigon and Timasheff, 1975b; Frigon, 1974) or with GDP (Howard and Timasheff, 1986; results). Then why should the Mg^{2+}-induced GDP-tubulin double rings dissociate upon warming? There could be several explanations—for instance, the difference in nucleotide exchange, or small differences in the solution conditions between the x-ray and the hydrodynamic studies—but we favor the following reasoning. Our results show that the formation of double rings made up of fully exchanged GDP-tubulin at increasing Mg^{2+} concentrations is accompanied by their aggregation into a pseudolattice, and that GTP back-exchange results in dissociation of both the pseudolattice and the double rings. Furthermore, upon warming a cold suspension of ring sheets, the x-ray scattering signals due to the double rings and their pseudolattice decay concomitantly. Therefore it is likely that the double rings are stabilized by their aggregation into a pseudolattice, that is, that ring formation and ring aggregation are linked equilibria (Wyman and Gill, 1990). In fact, we have not found conditions in which GDP-tubulin forms double rings without associating into ring arrays. Because the overall process is exothermic, whereas the tubulin association leading to ring formation is endothermic, the ring aggregation must be markedly exothermic. This resolves the apparent contradiction between the x-ray scattering and the sedimentation velocity studies. It is compatible with the fact that the protein surface regions involved in both associations are clearly different. Thus, whereas the linear association of tubulin molecules to form rings or microtubule protofilaments involves the ends of the tubulin $\alpha\beta$ heterodimer, the superposition of the outer rings of the pseudolattice involves contacts between lateral tubulin zones, which possibly correspond to the zones exposed in the outside and/or inside of the microtubule surface (Díaz et al., 1994). The situation is analogous to that of the tubulin rings formed together with microtubule-associated proteins (MAPs), which are less stable at 37°C than in the cold; even the formation of pure tubulin rings is endothermic (discussed by Melki et al., 1989). The dissociation of tubulin-MAP rings at warm temperatures was evidenced by x-ray solution scattering by Bordas et al. (1983), even though in that study the characteristically modulated J_0 maxima of double rings could not observed because of the limited resolution of the data.

Taxoid-induced microtubule assembly starting from double rings, tubulin oligomers, or tubulin dimers

Upon warming a suspension of GDP-tubulin double-ring aggregates in the presence of taxoid, the dissociation of the

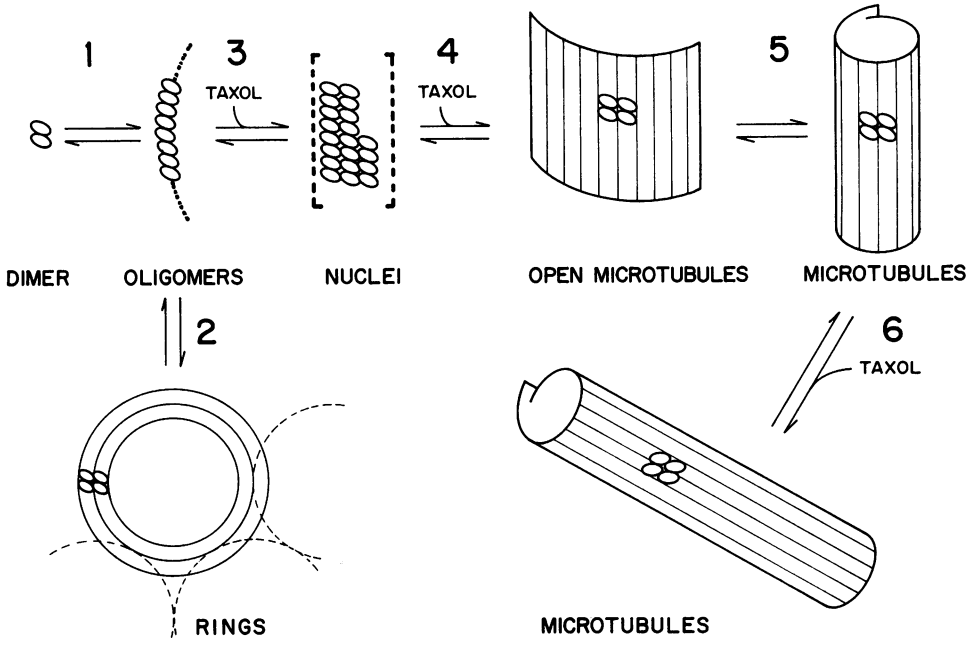

FIGURE 12 Scheme of the Mg^{2+}-induced self-association processes of GDP-tubulin to form double rings and taxoid-induced microtubules, characterized by time-resolved x-ray scattering. The tubulin dimer, oligomers, ring aggregates, open microtubules, and microtubules (without distinction of their length) have been identified by x-ray scattering in this work. The size and degree of curvature of oligomers are not known from the data, and the microtubule polymerization nuclei (in dashed brackets) have been inferred but have passed undetected.

rings is followed by the assembly of microtubules (compare Fig. 7 *B* to Fig. 6 *B*). However, residual double rings remain, and at high Mg^{2+} concentrations the formation of the double-ring aggregates actually blocks microtubule assembly. In these conditions ring and microtubule scattering maxima overlap, and the species from which microtubules are assembled cannot be easily characterized. This situation is analogous to that previously encountered with solutions of tubulin plus microtubule-associated proteins, in which the ring disassembly overlaps with microtubule assembly (Bordas et al., 1983; Spann et al., 1987). Thus, the formation of double-ring aggregates is a process that competes with microtubule assembly. As previously pointed out (Timasheff, 1991), ring assembly is favored in the GDP-bound form of tubulin. With our approach the masking of the assembly pathways due to the presence of rings is easily avoided, because the back-exchange of GTP into its binding site reduces the formation of double rings and delivers solutions of GTP-tubulin with a majority of linear oligomers (Fig. 5). Assembly of GTP-tubulin oligomers into microtubules is then induced by taxol (Fig. 9). The simplest assumption is that the oligomeric products of ring disassembly (*reverse process 2* in Fig. 12) are essentially the same as the initial oligomers that lead to microtubule assembly (*processes 3* and beyond in Fig. 12). Assembly of microtubules can also be accomplished from pure (GDP or GTP bound) tubulin dimers by isothermal addition of $MgCl_2$ in the presence of taxol (Fig. 8), that is, via processes from 1 and 3, to 6 in the scheme of Fig. 12.

Two-dimensional intermediate species in microtubule assembly

Microtubular sheets have frequently been observed in electron micrographs of negatively stained microtubule preparations (Erickson, 1974; figure 5 in Andreu et al., 1994), and their kinetic accumulation in solution appears to be the cause of a characteristic turbidity overshoot observed under certain conditions (Detrich et al., 1985). Microtubular sheets have also been observed by cryoelectron microscopy in unstained samples (see Fig. 8 in Andreu et al., 1992). Nevertheless, it could be argued that the presence of the microtubular sheets is due to preparative sample artifacts. However, our data here show that the assembly in solutions containing 40% GDP tubulin showed a short lag (nucleation phase), followed by the formation of open microtubule walls and their subsequent closure into microtubules (Fig. 10). This pathway is represented by processes 4 and 5 in the scheme shown in Fig. 12. The fact that open microtubules constitute a fraction of the structures present in the solution (*inset* in Fig. 10 *A*) provides direct structural evidence for the existence of these intermediate species in a unperturbed solution undergoing microtubule polymerization and gives proof of the bidimensional nature of microtubule growth. Although microtubules were first described as helical structures (Amos and Klug, 1974), the helical growth of microtubules is very unlikely. In fact, because they have lattice discontinuities at a seam, most of the microtubule cylindrical polymers are pseudohelical (Andreu et al., 1992; Kikkawa et al., 1994; Song and Mandelkow, 1995; Nojima et al., 1995). As in the observed formation and closure of microtubule sheets, it is conceivable that the end growth of microtubules is not helical but proceeds by one- or two-dimensional elongation followed by accretion into the pseudohelical lattice. Indeed, very recent cryoelectron microscopy studies of growing microtubule ends have reported the presence of two-dimensional sheets that close into tubes (Chrétien et al., 1995). It should be noted that the above does not contradict the fact that microtubules may also elongate by endwise addition, as indicated by process 6 in

the scheme of Fig. 12, and that microtubules may also associate end to end (Williams and Rone, 1989). In fact, these processes probably occur after short microtubules have been formed. This type of elongation cannot be followed by x-ray solution scattering because microtubules grow to lengths greater than the dimensions given by the lower-resolution cutoff of the data (Bordas et al., 1983).

Microtubule nucleation and the mechanisms of taxoid-tubulin interactions

The above prompts the question of how microtubule sheets form from tubulin oligomers. The simplest hypothesis is that the necessary bidimensional polymerization nuclei should form by accretion of linear tubulin oligomers induced by taxol, as indicated by process 3 in the scheme of Fig. 12. Such species are possibly transient and not necessarily homogeneous, and they should be present in small concentrations. Their structures are likely to range between those of open double-ring fragments (*solid line 4* in Fig. 3) and those of microtubule sheets (*lines 6* in Fig. 3). These characteristics diminish the possibility that they could be detected by time-resolved x-ray scattering, unless their growth into microtubule sheets could be slowed down. Nevertheless, we argue that microtubule nuclei are probably small two-dimensional fragments of the microtubule wall. This is because their growth produces open microtubules and because such structures are in agreement with theoretical principles of cooperative protein association (Erickson and Pantaloni, 1981). We believe that it is unlikely that the nuclei would be helical, because that would imply the previous formation of laterally bound oligomers and very short (one- or two-turn) microtubules. These would yield very characteristic scattering profiles, which have not been observed. The microtubule nucleation species could be biochemically detected if the binding of labeled taxol or docetaxel to tubulin oligomers (*process 3* in Fig. 12) was proved.

The effects of binding of taxoid and nucleoside triphosphate have interesting similarities and differences. The binding of both taxoid and nucleotide γ-phosphate stabilize microtubules. The nucleotide is exchangeable in the tubulin dimer but is nonexchangeable in assembled microtubules (Erickson and O'Brien, 1992). In contrast, the taxoid-binding site is undetectable in the free dimer, but readily accessible in microtubules (Parness and Horwitz, 1981; Dye et al., 1993; Díaz et al., 1993, and unpublished results). Both taxoid and the exchangeable nucleotide bind to β-tubulin, predominantly at its amino-terminal zone (Shivanna et al., 1993; Rao et al., 1994). Taxoid binding causes a small reproducible shift to lower angles in the position of the x-ray solution scattering maxima J_3 and J_{n-3} in the first layer line, indicating longer spacings (Andreu et al., 1994, and unpublished results). This is consistent with an increase in the monomer axial repeat of approximately 0.13 nm (Vale et al., 1994). It is known that taxoid binding changes the superstructure and flexural rigidity of microtubules (Dye et al., 1993; Venier et al., 1994; Mickey and Howard, 1995; Kurz and Williams, 1995). It is also known that binding of structural analogs of the γ-phosphate to GDP-microtubules increases their rigidity (Venier at al., 1994) and that microtubules assembled with the slowly hydrolyzable nucleotide analog GMPCPP are more rigid and have a 0.15 nm longer axial spacing between monomers than GDP-microtubules (Vale et al., 1994; Hyman et al., 1995). [It should be noted that microtubule thermodynamic stability, microtubule flexural rigidity, and microtubule axial spacing are being independently considered in this discussion.]

Rings are equivalent to adjacent microtubule protofilaments that are coiled tangent to the microtubule wall, with the tubulin dimers in a curved inactive conformation (Mandelkow et al., 1988; Melki et al., 1989; Díaz et al., 1994). The observation that taxol appears not to modify the ring formation equilibrium (Results) suggests, by application of the linked equilibria concepts (Wyman and Gill, 1990), that the rings as such bind the ligand no more or less than the tubulin dimer, which in fact binds taxoids nonsignificantly (Díaz et al., 1993). Therefore it appears that both the binding of taxoid to GDP-tubulin and that of the nucleotide γ-phosphate, even though they give nonidentical effects, are linked to the straight tubulin dimer conformation, which is active in microtubule assembly, as previously proposed (Díaz et al., 1993). The binding of the side chain of taxol leads to a reduction in the lateral bonding angle between tubulin molecules, which gives microtubules with one less protofilament than docetaxel-induced microtubules, and an excess taxoid induces microtubule opening (Andreu et al., 1994). This suggests that taxol binds between neighboring protofilaments. It has been shown by subtraction of electron micrographs of zinc-induced tubulin sheets with and without taxol that one taxol binding site per tubulin dimer is placed between protofilaments (Nogales et al., 1995). However, zinc-induced tubulin sheets have an inverted protofilament topology with respect to microtubules. If part of the taxoid-tubulin contacts in these zinc sheets were similar to those in microtubules, taxol would bind between microtubule protofilaments. An important open question is how taxol binding favors the active tubulin conformation. This may be either because an allosteric mechanism takes place in which taxoid binding to a distant site may change the lateral interactions and the shape of tubulin (Dye et al., 1993; Derry et al., 1995) or because the taxoid-binding site may be constituted by a lateral bonding interface between adjacent tubulin molecules in the microtubule, for example, in the grooves between protofilaments, and straight conformation could be a simple result of the protofilament accretion (Howard and Timasheff, 1986; Andreu et al., 1992; Díaz et al., 1993; Andreu et al., 1994).

We thank E. Nogales and F. J. Medrano for their help during x-ray measurements, E. Pantos for providing the codes to calculate the scattering simulation, P. Usobiaga for analytical ultracentrifugation, and M. Menendez for discussion.

This work was supported by DGICyT grants PB900303 and PB920007 and the EU Large Installations Program.

REFERENCES

Amos, L. A., and A. Klug. 1974. Arrangement of subunits in flagellar microtubules. *J. Cell Sci.* 14: 523–549.

Andreu, J. M., J. Bordas, J. F. Díaz, J. García de Ancos, R. Gil R., F. J. Medrano, E. Nogales, E. Pantos., and E. Towns-Andrews. 1992. Low resolution structure of microtubules in solution. Synchrotron x-ray scattering and electron microscopy of taxol-induced microtubules assembled from purified tubulin in comparison with glycerol- and Map-induced microtubules. *J. Mol. Biol.* 226:169–184.

Andreu, J. M., J. F. Díaz, R. Gil, J. M. de Pereda, M. García de Lacoba, V. Peyrot, C. Briand, E. Towns-Andrews, and J. Bordas. 1994. Solution structure of taxotere-induced microtubules to 3 nm resolution. The change in protofilament number is linked to the binding of the taxol side chain. *J. Biol. Chem.* 269:31785–31792.

Andreu, J. M., J. García de Ancos, D. Starling, J. L. Hodgkinson, and J. Bordas. 1989. A synchrotron X-ray scattering characterization of purified tubulin and of its expansion induced by mild detergent binding. *Biochemistry.* 28:4036–4040.

Beese, L., G. Stubbs, and C. Cohen. 1987. Microtubule structure at 18 Å resolution. *J. Mol. Biol.* 194:257–264.

Bollag, D. M., P. A. McQueeney, J. Zhu, O. Hensens, L. Koupal, J. Liesch, E. Lazarides, and C. M. Woods. 1995. Epothilones, a new class of microtubule- stabilizing agents with a taxol-like mechanism of action. *Cancer Res.* 55:2325- 2333.

Bordas, J., E. M. Mandelkow, and E. Mandelkow. 1983. Stages of tubulin assembly and disassembly studied by time-resolved synchrotron x-ray scattering. *J. Mol. Biol.* 164:89–135.

Butner, K. A., and M. W. Kirschner. 1991. Tau protein binds to microtubules through a flexible array of distributed weak sites. *J. Cell Biol.* 115:717–730.

Chretién, D., S. D. Fuller, and E. Karsenti. 1995. Structure of growing microtubule ends: two-dimensional sheets close into tubes at variable rates. *J. Cell. Biol.* 129:1311–1328

Derry, W. B., L. Wilson, and M. A. Jordan. 1995. Substoichiometric binding of taxol supresses microtubule dynamics. *Biochemistry.* 34: 2203–2211.

Detrich, H. W., M. A. Jordan, L. Wilson, and R. C. Williams. 1985. Mechanism of microtubule assembly. Changes in polymer structure and organization during assembly of sea urchin egg tubulin. *J. Biol. Chem.* 260:9479–9490.

Díaz, J. F., and J. M. Andreu. 1993. Assembly of purified GDP-tubulin into microtubules induced by taxol and taxotere: reversibility, ligand stoichiometry and competiton. *Biochemistry.* 32:2747–2755.

Díaz, J. F., M. Menendez, and J. M. Andreu. 1993. Thermodynamics of ligand induced assembly of tubulin. *Biochemistry.* 32:10067–10077.

Díaz, J. F., E. Pantos, J. Bordas, and J. M. Andreu. 1994. Solution structure of GDP-tubulin double rings to 3 nm resolution and comparison with microtubules. *J. Mol. Biol.* 238:214–223.

Dreschel, D. N., and M. W. Kirschner. 1994. The minimum GTP cap required to stabilize microtubules. *Curr. Biol.* 4:1053–1061.

Dye, R. B., S. P. Fink, and R. C. Williams. 1993. Taxol-induced flexibility of microtubules and its reversal by Map-2 and Tau. *J. Biol. Chem.* 268:6847–6850.

Erickson, H. P. 1974. Microtubule surface lattice and subunit structure and observations on reassembly. *J. Cell Biol.* 60:153–167

Erickson, H. P., and E. T. O'Brien. 1992. Microtubule dynamic instability and GTP hydrolysis. *Annu. Rev. Biophys. Biomol. Struct.* 21:145–166.

Erickson, H. P., and D. Pantaloni. 1981. The role of subunit entropy in cooperative assembly. Nucleation of microtubules and other two-dimensional polymers. *Biophys. J.* 34:293–309.

Frigon, R. P. 1974. Ph.D. thesis. Brandeis University.

Frigon, R. P., and S. N. Timasheff. 1975a. Magnesium-induced self-asociation of calf brain tubulin. I. Stoichiometry. *Biochemistry.* 14: 4559–4566.

Frigon, R. P., and S. N. Timasheff. 1975b. Magnesium-induced self-association of calf brain tubulin. II. Thermodynamics. *Biochemistry.* 14:4567–4573.

García de la Torre, J., and J. M. Andreu. 1994. Hydrodynamic analysis of tubulin dimer and double rings. *J. Mol. Biol.* 238:223–225.

Gilbert, S. P., M. R. Webb, M. Brune, and K. A. Johnson. 1995. Pathway of processive ATP hydrolysis by kinesin. *Nature.* 373:671–676

Hirose, K., A. Lockhart, R. A. Cross, and L. A. Amos. 1995. Nucleotide-dependent angular change in kinesin motor domain bound to tubulin. *Nature.* 376:277–279.

Hoenger, A., E. P. Sablin, R. D. Vale, R. J. Fletterick, and R. A. Milligan. 1995. Three-dimensional structure of a tubulin-motor-protein complex. *Nature.* 376:271–274.

Horwitz, S. B. 1994. How to make taxol from scratch. *Nature.* 367: 593–594.

Howard, W. D., and S. N. Timasheff. 1986. GDP state of tubulin: stabilization of double rings. *Biochemistry.* 25:8292–8300.

Hyams, J. S., and C. W. Lloyd. 1994. Microtubules. Wiley-Liss, New York.

Hyman, A. A., D. Chretien, I. Arnal, and R. H. Wade. 1995. Structural changes accompanying GTP hydrolyisis in microtubules: information from a slowly hydrolyzable analogue GMPCPP. *J. Cell Biol.* 128: 117–125.

Kikkawa, M., T. Ishikawa, T. Nakata, T. Wakabayashi, and N. Hirokawa. 1994. Direct visualization of the microtubule lattice seam both in vitro and in vivo. *J. Cell. Biol.* 127:1965–1971.

Kikkawa, M., T. Ishikawa, T. Wakabayashi, and N. Hirokawa. 1995. Three-dimensional structure of the kinesin head-microtubule complex. *Nature.* 376:274–277.

Kingston, D. G. 1994. Taxol: the chemistry and structure-activity relationships of a novel anticancer agent. *Trends Biotechnol.* 12:222–227.

Kurz, J. C., and Williams, R. C. 1995. Microtubule-associated proteins and the flexibility of microtubules. *Biochemistry.* 34:13374–13380.

Lee, J. C., and S. N. Timasheff. 1975. The reconstitution of microtubules from purified calf brain tubulin. *Biochemistry.* 14:5183–5187.

Mandelkow, E. M., G. Lange, A. Jagla, U. Spann, and E. Mandelkow. 1988. Dynamics of the microtubule oscillator: role of nucleotides and tubulin-MAP interactions. *EMBO J.* 7:357–365.

Mandelkow, E., and E. Mandelkow. 1995. Microtubules and microtubule-associated proteins. *Curr. Opin. Cell Biol.* 7:72–81.

Martin, S. R., M. J. Schlistra, and P. M. Bayley. 1993. Dynamic instability of microtubules: Monte Carlo simulation and application to different types of microtubule lattice. *Biophys. J.* 65:578–596.

Melki, R., M. F. Carlier, and D. Pantaloni. 1988. Oscillations in microtubule polymerization: the rate of GTP regeneration on tubulin controls the period. *EMBO J.* 7:2653–2659.

Melki, R., M. F. Carlier, D. Pantaloni, and S. N. Timasheff. 1989. Cold depolymerization of microtubules to double rings: geometric stabilization of assemblies. *Biochemistry.* 28:9143–9152.

Mickey, B., and J. Howard. 1995. Rigidity of microtubules is increased by stabilizing agents. *J. Cell Biol.* 130:909–917.

Nogales, E., S. G. Wolff, I. A. Khan, R. F. Ludueña, and K. H. Downing. 1995. Structure of tubulin at 6.5 Å and location of the taxol binding site. *Nature.* 375:424–427.

Nojima, D., R. W. Linck, and E. H. Egelman. 1995. At least one of the protofilaments in flagellar microtubules is not composed of tubulin. *Curr. Biol.* 5:158–167.

Novella, I. S., J. M. Andreu, and D. Andreu. 1992. Chemically synthesized 182–235 segment of Tau protein and analogue peptides are efficient in vitro microtubule assembly inducers of low apparent sequence specificity. *FEBS Lett.* 3:235–240.

Oosawa, F., and S. Asakura. 1975. Thermodynamics of the Polymerization of Protein. Academic Press, London.

Pantos, E., and J. Bordas. 1994. Supercomputer simulation of small angle x-ray scattering, electron micrographs and x-ray diffraction patterns of macromolecular strructures. *J. Pure Appl. Chem.* 66:77–82.

Parness, J., and S. B. Horwitz. 1981. Taxol binds to polymerized tubulin in vitro. *J. Cell. Biol.* 91:479–487.

Rao, S., N. E. Krauss, J. M. Heerding, C. S. Swindell, I. Ringel, G. A. Orr, and S. B. Horwitz. 1994. 3′-(*p*-Azidobenzamido)taxol photolabels the N-terminal 31 aminoacids of β-tubulin. *J. Biol. Chem.* 269:3132–3134.

Rowinsky, E. K., and R. C. Donehower. 1995. Paclitaxel (Taxol). *N. Engl. J. Med.* 332:1004–1014.

Shearwin, K. E., and S. N. Timasheff. 1992. Linkage between ligand binding and control of tubulin conformation. *Biochemistry.* 33:885–893.

Shivanna, B. D., M. R. Mejillano, T. D. Williams, and R. Himes. 1993. Exchangeable GTP site of β-tubulin. *J. Biol. Chem.* 268:127–132.

Song, Y. H., and E. Mandelkow. 1995. The anatomy of flagellar microtubules: polarity, seam, junctions and lattice. *J. Cell Biol.* 128:81–94

Spann, U., W. Renner, E. M. Mandelkow, J. Bordas, and E. Mandelkow. 1987. Tubulin oligomers, and microtubule assembly studied by time-resolved x-ray scattering: separation of prenucleation, and nucleation events. *Biochemistry.* 26:1123–1132.

Timasheff, S. N. 1991. The role of double rings in the tubulin-microtubule cycle: linkage with nucleotide binding. *Am. Inst. Phys. Conf. Proc.* 226:170–180.

Vale, R. D., C. M. Coppin, F. Malik, F. J. Kull, and R. A. Milligan. 1994. Tubulin GTP hydrolysis influences the structure, mechanical properties and kinesin-driven transport of microtubules. *J. Biol. Chem.* 269: 23769–23775.

Venier, P., A. C. Maggs, M. F. Carlier, and D. Pantaloni. 1994. Analysis of microtubule rigidity using hydrodynamic flow and thermal fluctuations. *J. Biol. Chem.* 269:13353–13360.

Williams, R., and L. A. Rone. 1989. End-to-end joining of taxol-stabilized GDP-containing microtubules. *J. Biol. Chem.* 264:1663–1670.

Wyman, J, and S. J. Gill. 1990. Binding and Linkage. University Science Books, Mill Valley, CA.